C. R. Mecanique 345 (2017) 735–741

Contents lists available at ScienceDirect

Comptes Rendus Mecanique

www.sciencedirect.com

Geometrical versus rheological transient creep closure in a salt cavern

Pierre Bérest [a,*], Mehdi Karimi-Jafari [a,1], Benoît Brouard [b]

[a] Laboratoire de mécanique des solides, École polytechnique, route de Saclay, 91128 Palaiseau cedex, France
[b] Brouard Consulting, 101, rue du Temple, 75003 Paris, France

ARTICLE INFO

Article history:
Received 27 June 2017
Accepted 4 September 2017
Available online 28 September 2017

Keywords:
Creep
Reverse creep
Salt caverns
In situ tests

ABSTRACT

An in-situ test performed in a brine-filled cavern proves that, when brine pressure decreases rapidly, the creep closure rate increases drastically. Conversely, a rapid pressure increase leads to "reverse" creep closure: cavern volume increases, even when, at cavern depth, fluid pressure is lower than geostatic pressure. It is tempting to explain these two phenomena by transient salt creep, a characteristic feature of salt rheological behavior commonly observed during laboratory creep tests. In fact, computations performed on an idealized cylindrical cavern excavated from a Norton–Hoff rock mass (a constitutive law that includes no transient component) prove that these two phenomena are, at least partly, of a structural nature: their origin is in the slow redistribution of stresses following any pressure change.

1. Field and laboratory evidence

1.1. An in-situ test performed in a salt cavern

An "outflow" test was performed by Hugout [1] in a cavern leached out from a salt formation during the spring of 1982 at Étrez, France, where the utility company Storengy operates an underground gas-storage facility. Cavern depth and height were 950 m and 50 m, respectively, and cavern volume is $V = 7,500 \pm 500$ m^3. After leaching was completed, well completion included a central string filled with saturated brine with a volumetric weight of $\gamma_b = 0.012$ MPa/m and an annular space filled with oil of volumetric weight $\gamma_o = 0.0085$ MPa/m. The brine/oil interface in the cavern was approximately $H = 950$ m deep, at which depth geostatic pressure is $P_\infty = \gamma_R H = 20.9$ MPa when $\gamma_R = 0.022$ MPa/m. At the wellhead, brine pressure was zero; cavern pressure was $P_\infty - \Delta P = \gamma_b H = 11.4$ MPa, and oil pressure was $\delta P = (\gamma_b - \gamma_o)\, H = 3.4$ MPa (Fig. 1).

On September 8, 1982, 93 days after leaching completion, the brine outflow rate was slightly more than 100 l/day (Fig. 2). The main driving forces for brine outflow were cavern-creep closure and brine warming. (During cavern solution-mining, soft water was pumped from a shallow aquifer and injected into the cavern. The injected water was significantly colder than the rock mass at a 950-m depth; after leaching was completed, cavern brine slowly warms and expands.) The valve on the annular space was opened rapidly, resulting in a cavern-pressure drop from $P_\infty - \Delta P = 11.4$ MPa to $P_\infty - \Delta P - \delta P = 8$ MPa.

* Corresponding author.
E-mail address: berest@lms.polytechnique.fr (P. Bérest).
[1] Now with Geostock, Rueil Malmaison, France.

http://dx.doi.org/10.1016/j.crme.2017.09.002

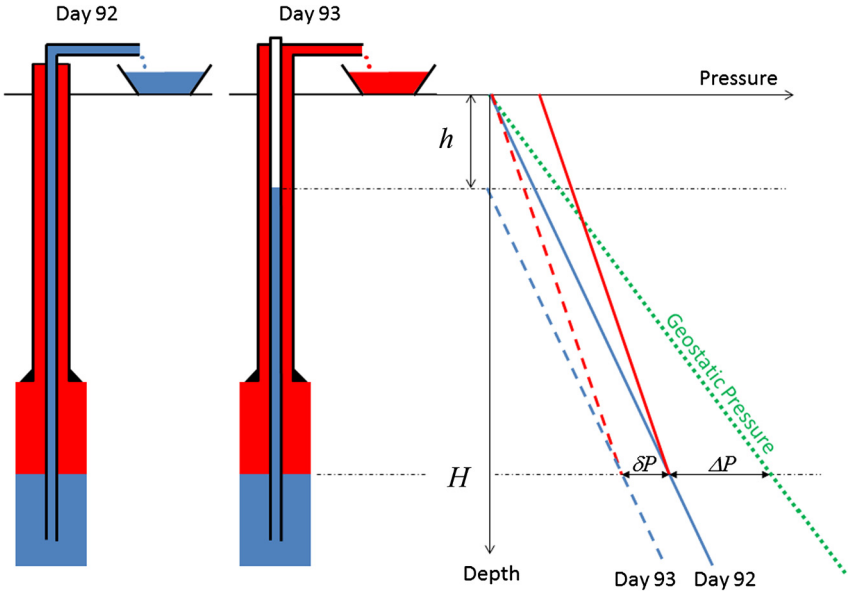

Fig. 1. Distribution of fluid pressures during the two phases of the test.

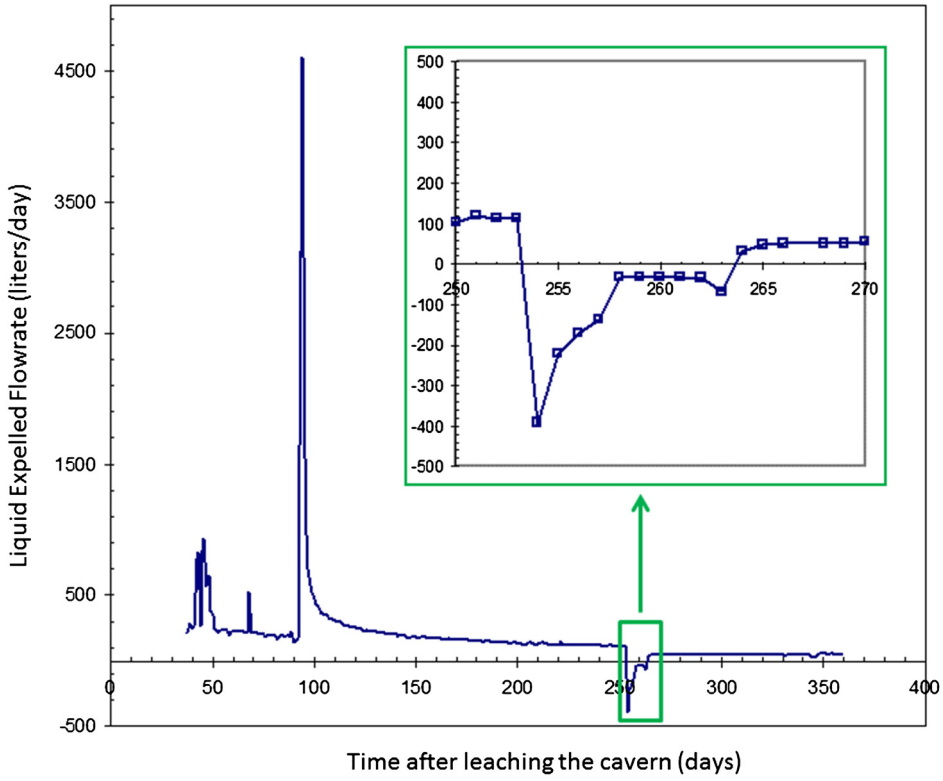

Fig. 2. Fluid flowrate expelled during the test (after [1]).

In the central string, the brine–air interface dropped by $h = (\gamma_b - \gamma_o)\, H/\gamma_b = 290$ m (Fig. 1). The hydrocarbon outflow rate was measured from Day 93 to Day 360 (Fig. 2). The rate was 4500 l/day for a couple of days after the Day 93 cavern-pressure drop, after which it declined rapidly.

On Day 253, the annular space was closed, and brine was injected in the central string to restore the Day 92 configuration (Fig. 1). Cavern pressure increased from $P_\infty - \Delta P - \delta P = 8$ MPa to $P_\infty - \Delta P = 11.4$ MPa. For 12 days, the brine level consistently *dropped* in the central tubing (the flow rate of the brine was negative), and additional brine was injected to

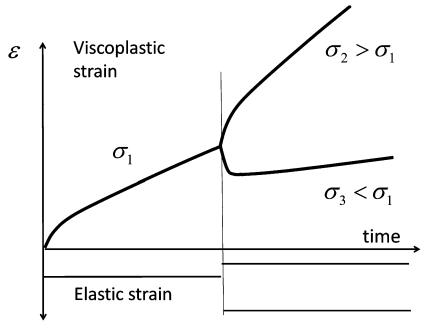

Fig. 3. Creep test on a salt sample: after some time, the applied load (σ_1) is increased to σ_2 or decreased to σ_3.

keep the air–brine interface at ground level. This apparent cavern volume increase was due to several factors, among which the most important is additional dissolution (salt concentration at saturation is an increasing function of brine pressure: when pressure increases, salt is dissolved at the cavern wall to reach chemical equilibrium; however, brine volume is smaller than the volumes of its constituents, resulting in a net cavern volume increase) and "reverse" cavern-creep closure. (Cavern volume increases, even though cavern pressure is *lower* than geostatic pressure.) These effects and several other minor phenomena triggered by the cavern pressure change – such as adiabatic brine warming – can be assessed precisely [2]. The cumulated brine volume injected in the cavern to compensate for cavern-volume increase during this 12-day period was 1077 l, of which, according to computations, 444 l were due to additional dissolution. After Day 265, a more or less constant brine-flow rate was observed. This rate was lower than the pre-test brine-flow rate, partly because brine warming was slower than it was before Day 93.

1.2. Laboratory creep tests

These changes in cavern closure rate are somewhat similar to what is observed during laboratory tests performed on salt samples when applied loads are changed, as schematically described in Fig. 3. At $t = 0$, a constant uniaxial load, $\sigma_1 > 0$, is applied to a cylindrical salt sample. (Compressive stresses and contractions are positive when describing the results of a laboratory test.) The immediate response to a load change is elastic; it can be described by a linear relation between strain and stress. It is followed by transient creep, described later. After some time (several months), a steady state is reached, and the strain rate remains constant. The steady-state rate is a non-linear function of deviatoric stress and temperature. The Norton–Hoff law, or $\dot{\varepsilon} = A(T)\sigma^n$, captures the main features of the steady-state behavior; it is not able to describe the transient behavior. In the case of rock salt, the mean stress has no influence on strain rate, and no volumetric change is observed.

Any change in applied load triggers transient creep. Following a load increase, $\sigma_2 > \sigma_1$, transient behavior is characterized by fast initial rates; following a load decrease, $\sigma_3 < \sigma_2$, transient behavior is characterized by slow initial rates, or even negative ("reverse") initial rates [3–5] – at least when the "stress drop" is large enough (Fig. 3). These transient rates slowly decrease or increase to reach steady-state values, as explained above.

It is tempting to infer that the effects observed during cavern testing (rapid creep closure when cavern pressure is lowered abruptly, "reverse" creep closure when pressure is increased) are a direct consequence of the transient behavior observed at the laboratory. It will be proved in the following that even the Norton–Hoff steady-state law is able to capture, at least to some extent, the effects observed in salt caverns, even though no transient component is taken into account in this constitutive law.

2. Transient behavior of an idealized cylindrical cavern in a Norton–Hoff medium

2.1. Cylindrical symmetry

The 3D generalization of the Norton–Hoff law can be written:

$$\dot{\varepsilon}_{ij} = \frac{1+\nu}{E}\dot{\sigma}_{ij} - \frac{\nu}{E}\dot{\sigma}_{kk}\delta_{ij} + \frac{3A}{2}\left(\sqrt{3J_2}\right)^{n-1} s_{ij} \tag{1}$$

(no transient behavior is taken into account, and temperature dependence is not mentioned), where σ_{ij} is the stress tensor, s_{ij} is the deviatoric stress tensor and $J_2 = s_{ij}s_{ji}/2$ is its second invariant, $\dot{\varepsilon}_{ij}$ is the strain rate tensor, and ν, E, A and n are four constants (when temperature is kept constant) – $n = 3$ to 5 is typical. Note that Eq. (1) predicts that, during a uniaxial creep test, $|\dot{\varepsilon}_{zz}| = A\,|\sigma_{zz}|^n$, as mentioned in Section 1.2. The elastic component of the strain rate depends on the mean stress; however, this dependency will vanish in the following when $\nu = 0.5$ is assumed.

An idealized, infinite, cylindrical cavern of radius a is considered. Taking into account cylindrical symmetry and plane strain conditions, the constitutive law (2), (3) and (4), the equilibrium condition (5), the boundary condition (6) and the initial conditions (7) can be written as follows:

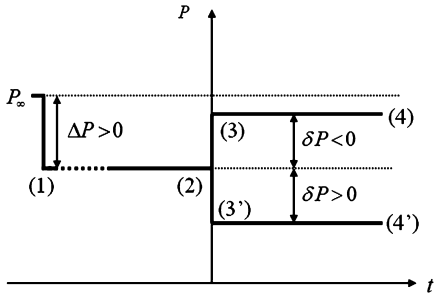

Fig. 4. Cavern pressure changes.

$$\frac{\partial \dot{u}}{\partial r} = \frac{\dot{\sigma}_{rr} - \nu\left(\dot{\sigma}_{\varphi\varphi} + \dot{\sigma}_{zz}\right)}{E} + A\sqrt{3J_2}^{n-1}\frac{2\sigma_{rr} - \sigma_{\varphi\varphi} - \sigma_{zz}}{2} \tag{2}$$

$$\frac{\dot{u}}{r} = \frac{\dot{\sigma}_{\varphi\varphi} - \nu\left(\dot{\sigma}_{zz} + \dot{\sigma}_{rr}\right)}{E} + A\sqrt{3J_2}^{n-1}\frac{2\sigma_{\varphi\varphi} - \sigma_{zz} - \sigma_{rr}}{2} \tag{3}$$

$$0 = \frac{\dot{\sigma}_{zz} - \nu\left(\dot{\sigma}_{rr} + \dot{\sigma}_{\varphi\varphi}\right)}{E} + A\sqrt{3J_2}^{n-1}\frac{2\sigma_{zz} - \sigma_{rr} - \sigma_{\varphi\varphi}}{2} \tag{4}$$

$$r\frac{\partial \sigma_{rr}(r,t)}{\partial r} + \sigma_{rr}(r,t) - \sigma_{\varphi\varphi}(r,t) = 0 \tag{5}$$

$$\sigma_{rr}(a,t) = -P_c(t) \tag{6}$$

$$\sigma_{rr}(r,\infty) = \sigma_{\varphi\varphi}(r,\infty) = \sigma_{zz}(r,\infty) = -P_\infty \tag{7}$$

where $\sigma_{rr}(r,t), \sigma_{\varphi\varphi}(r,t), \sigma_{zz}(r,t)$ are the radial, tangential and axial stresses, respectively; $\dot{u} = \dot{u}(r,t)$ is the radial displacement rate; cavern pressure is $P_c = P_c(t)$, and $P_\infty > P_c$ is the geostatic pressure. Only small strains and displacements are considered. For simplicity, $\nu = 0.5$ is assumed, from which it can be inferred that, at any time, $2\sigma_{zz} = \sigma_{rr} + \sigma_{\varphi\varphi}$, $\sqrt{3J_2} = |\sigma_{rr} - \sigma_{\varphi\varphi}|$, and $\dot{u}/r = a\dot{a}/r^2$, when $\dot{a}$ is the displacement rate at the cavern's wall. Eq. (3) can be rewritten:

$$\frac{a\dot{a}(t)}{r^2} = \frac{3r}{4E}\frac{\partial \dot{\sigma}_{rr}(r,t)}{\partial r} + \frac{A\sqrt{3}}{2}\left|\frac{-r}{2}\frac{\partial \sigma_{rr}(r,t)}{\partial r}\right|^{n-1}\frac{r}{2}\frac{\partial \sigma_{rr}(r,t)}{\partial r} \tag{8}$$

2.2. Steady-state creep closure

When cavern pressure is kept constant ($P_\infty - P_c = \Delta P > 0$), steady state is reached after an infinite period of time. In such a state, the derivatives of stresses with respect to time vanish. Eq. (8) can be divided by r and integrated with respect to r between $r = a$ and $r = \infty$, leading to

$$\frac{\dot{a}_{ss}}{a} = -\frac{\sqrt{3}^{n+1}}{2}A^*\left(\frac{\Delta P}{n}\right)^n \tag{9}$$

and the steady-state stress distribution is

$$\sigma_{rr}^{ss}(r) = -P_\infty + \Delta P\left(\frac{a}{r}\right)^{2/n}\sigma_{\varphi\varphi}^{ss}(r) = -P_\infty + \left(1 - \frac{2}{n}\right)\Delta P\left(\frac{a}{r}\right)^{2/n}\sigma_{zz}^{ss}(r) = -P_\infty + \left(1 - \frac{1}{n}\right)\Delta P\left(\frac{a}{r}\right)^{2/n} \tag{10}$$

In the following, in order to avoid handling cumbersome equations, it is assumed that $n = 3$ or 5; however, the method explained below can be applied to any value of n. Taking into account Eq. (9), Eq. (8) can be rewritten as

$$\frac{a\dot{a}(t)}{r^2} = \frac{3r}{4E}\frac{\partial \dot{\sigma}_{rr}(r,t)}{\partial r} + \frac{\dot{a}_{ss}}{a}\left[\frac{-nr}{2\Delta P}\frac{\partial \sigma_{rr}(r,t)}{\partial r}\right]^n \tag{11}$$

2.3. Initial transient behavior after a swift cavern pressure closure

It is assumed now that a constant pressure $P_c = P_\infty - \Delta P$ was applied in the cavern over a long period of time, $-\infty < t < 0$, and that steady state was reached at $t = 0^-$. At $t = 0$, cavern pressure is changed abruptly, and cavern pressure becomes $P_c(t > 0) = P_\infty - \Delta P - \delta P$ (Fig. 4), where δP is > 0 or < 0.

2.4. Transient cavern volume rate

At $t = 0$, stress distribution experiences an elastic (instantaneous) change by

$$\delta\sigma_{rr}^{\mathrm{el}}(r,0^+) = \delta P\left(\frac{a}{r}\right)^2 \quad \delta\sigma_{\varphi\varphi}^{\mathrm{el}}(r,0^+) = -\delta P\left(\frac{a}{r}\right)^2 \quad \delta\sigma_{zz}^{\mathrm{el}}(r,0^+) = 0 \tag{12}$$

At $t = 0^+$, Eq. (11) writes

$$\frac{a\dot{a}(0^+)}{r^2} = \frac{3r}{4E}\frac{\partial\dot{\sigma}_{rr}(r,0^+)}{\partial r} + \frac{\dot{a}_{\mathrm{ss}}(0^-)}{a}\left[\frac{n\delta P}{\Delta P}\left(\frac{a}{r}\right)^2 + \left(\frac{a}{r}\right)^{\frac{2}{n}}\right]^n \tag{13}$$

This equation can be integrated numerically with respect to r. However, when n is an integer, this equation can be written

$$\frac{a\dot{a}(0^+)}{r^3} = \frac{3}{4E}\frac{\partial\dot{\sigma}_{rr}(r,0^+)}{\partial r} + \frac{\dot{a}_{\mathrm{ss}}(0^-)}{a}\frac{1}{r}\sum_0^n C_n^p\left(\frac{n\delta P}{\Delta P}\right)^p\left(\frac{a}{r}\right)^{2p+2(n-p)/n} \tag{14}$$

where C_n^p are the binomial coefficients. It can be integrated with respect to r between r and ∞, where the radial stress is constant:

$$-\frac{a\dot{a}(0^+)}{2r^3} = \frac{3}{4E}\dot{\sigma}_{rr}(r,0^+) - \frac{\dot{a}_{\mathrm{ss}}(0^-)}{a}\sum_0^n \frac{C_n^p}{2p+2(n-p)/n}\left(\frac{n\delta P}{\Delta P}\right)^p\left(\frac{a}{r}\right)^{2p+2(n-p)/n} \tag{15}$$

In particular, at $r = a$, $\dot{\sigma}_{rr}(a)|_{t=0+} = 0$, as cavern pressure is kept constant, and it can be inferred that

$$\frac{\dot{a}(0^+)}{\dot{a}_{\mathrm{ss}}(0^-)} = \sum_0^n \frac{nC_n^p}{np+n-p}\left(\frac{n\delta P}{\Delta P}\right)^p \tag{16}$$

Two features (which were not included in the constitutive law) then appear.

1. Following a pressure drop ($\delta P > 0$), the transient creep closure rate, $\dot{a}(0^+)$, is much faster than the steady-state rate, $\dot{a}_{ss}(0^-)$, observed before a cavern pressure drop.
2. Following a pressure increase ($\delta P < 0$), the "reverse" creep-closure rate, $\left(\dot{a}(0^+)/\dot{a}_{\mathrm{ss}}(0^-) < 0\right)$, can be observed after an increase in cavern pressure provided that the pressure increase is large enough.

When $n = 3$ and $n = 5$ (values often met in practice), the following formula hold:

$$n=3: \quad \frac{\dot{V}(0^+)}{\dot{V}_{\mathrm{ss}}(0^-)} = \frac{\dot{a}(0^+)}{\dot{a}(0^-)} = 1 + \frac{27}{5}\left(\frac{\delta P}{\Delta P}\right) + \frac{81}{7}\left(\frac{\delta P}{\Delta P}\right)^2 + 9\left(\frac{\delta P}{\Delta P}\right)^3$$

$$n=4: \quad \frac{\dot{V}(0^+)}{\dot{V}_{\mathrm{ss}}(0^-)} = \frac{\dot{a}(0^+)}{\dot{a}(0^-)} = 1 + \frac{125}{24}\left(\frac{\delta P}{\Delta P}\right) + \frac{1250}{13}\left(\frac{\delta P}{\Delta P}\right)^2 + \frac{6250}{17}\left(\frac{\delta P}{\Delta P}\right)^3 + \frac{15625}{21}\left(\frac{\delta P}{\Delta P}\right)^4 + 625\left(\frac{\delta P}{\Delta P}\right)^5$$

Also, the change in volume rate can be negative when the cavern experiences a large enough pressure increase ($\delta P < 0$). The case $n = 3$ is represented in Fig. 5. When $\delta P/\Delta P = 1$, the creep closure rate is multiplied by a factor of approximately 27; when $\delta P/\Delta P < -0.58$, reverse creep appears, and the cavern volume increases.

The case $n = 5$ is represented on Fig. 6. When $\delta P/\Delta P = 1$, the creep-closure rate is multiplied by a factor of approximately 1800; when $\delta P/\Delta P < -0.62$, reverse creep appears, and the cavern volume increases.

Note that in the case of the Étrez cavern, described in Section 1.1, $\delta P/\Delta P \simeq -0.36$, suggesting that the exponent of the power law is smaller than $n = 3$ – or that some other effects, not included in the model (e.g., transient creep) play a significant role.

2.5. Higher derivatives of displacement at the cavern wall

This method allows computing all derivatives of a with respect to time at $t = 0$. Computations are complex when higher derivatives are considered. For instance, the second derivative with respect to time can be inferred from Eq. (11):

$$\frac{a\ddot{a}(0^+)}{r^2} = \frac{3}{4E}\frac{r\partial\ddot{\sigma}_{rr}(r,0^+)}{\partial r} + \frac{\dot{a}_{\mathrm{ss}}(0^-)}{a}n\left(-\frac{n}{2\Delta P}\frac{r\partial\sigma_{rr}}{P\partial r}\right)^{n-1}\left(-\frac{n}{2\Delta P}\frac{r\partial\dot{\sigma}_{rr}}{P\partial r}\right) \tag{17}$$

or, using Eq. (11) again:

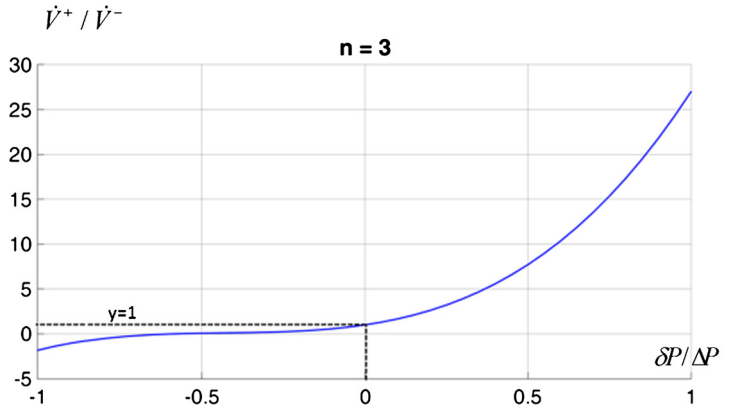

Fig. 5. Cavern creep closure increase (or decrease) as a function of fluid pressure increase ($n = 3$).

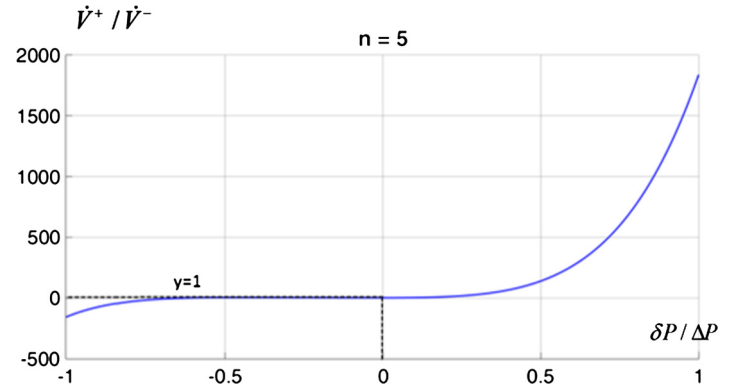

Fig. 6. Cavern creep closure increase (or decrease) as a function of fluid pressure increase ($n = 5$).

$$\frac{a\ddot{a}_{tr}(0^+)}{r^2} = \frac{3r\partial\ddot{\sigma}_{rr}(r,0^+)}{4E\partial r} - \ldots$$
$$\ldots\frac{2En^2}{3\Delta P}\frac{\dot{a}_{ss}^2(0^-)}{a^2}\left[\left(\frac{a}{r}\right)^{2/n} + n\frac{\delta P}{\Delta P}\left(\frac{a}{r}\right)^2\right]^{n-1}\left\{\frac{a^2}{r^2}\left[\sum_0^n \frac{nC_n^p}{np+n-p}\left(\frac{n\delta P}{\Delta P}\right)^p\right] - \left[\frac{n\delta P}{\Delta P}\left(\frac{a}{r}\right)^2 + \left(\frac{a}{r}\right)^{2/n}\right]^n\right\}$$

This equation can be divided by r and integrated with respect to r, leading to

$$-\frac{1}{2}\frac{a\ddot{a}(0^+)}{r^2} = \frac{3\dot{\sigma}_{rr}(r,0^+)}{4E} - \ldots$$
$$\ldots\frac{2En^2}{3\Delta P}\left(\frac{\dot{a}_{ss}(0^-)}{a}\right)^2\left[\begin{array}{l}\displaystyle\sum_0^{2n-1}\frac{C_{2n-1}^q\left(n\frac{\delta P}{\Delta P}\right)^q}{2(n-q)/n+2q}\left(\frac{a}{r}\right)^{2(n-q)/n+2q} - \ldots \\ \ldots\left[\displaystyle\sum_0^n\frac{nC_n^p}{np+n-p}\left(\frac{n\delta P}{\Delta P}\right)^p\right]\displaystyle\sum_0^n\frac{C_{n-1}^r\left(n\frac{\delta P}{\Delta P}\right)^r}{2+2r+2(n-1-r)/n}\left(\frac{a}{r}\right)^{2(n-1-r)/n+2r+2}\end{array}\right]$$

and when $r = a$,

$$\frac{\ddot{a}(0^+)}{a} = \frac{4En^2}{3\Delta P}\frac{\dot{a}_{ss}^2(0^-)}{a}\left[\sum_0^{2n-1}\frac{nC_{2n-1}^q\left(n\frac{\delta P}{\Delta P}\right)^q}{2\,(2n-1-q)+2nq} - \left[\sum_0^n\frac{nC_n^p}{np+n-p}\left(\frac{n\delta P}{\Delta P}\right)^p\right]\left[\sum_0^{n-1}\frac{nC_{n-1}^r}{4n+2nr-2-2r}\left(n\frac{\delta P}{\Delta P}\right)^r\right]\right]$$

As expected, when $n = 1$ (linear viscoelasticity), the second derivative vanishes to zero as the steady-state stress distribution is reached immediately after the pressure drop.

3. Conclusion

It has been proven that, after an abrupt pressure drop or pressure increase, an idealized cylindrical cavern created in an elastoviscoplastic Norton–Hoff infinite rock mass experiences a transient volume change, even when the constitutive law does not include a transient component. Reverse creep (cavern volume increase) can be observed following an increase in cavern pressure, even when it remains lower than geostatic pressure. This effect is due to the slow stress redistribution following the pressure change rather than to any *transient* creep behavior.

When transient convergence is observed in a tunnel (the convergence rate slowly decreases), it cannot be inferred that the constitutive viscoplastic law of the rock mass includes a transient component. Obviously, in an actual cavern or tunnel, in addition to this structural, or "geometrical", transient behavior, true "rheological" transient behavior can play a significant role.

Acknowledgements

The authors are indebted to Sivaprasath Manivannan and Kathy Sikora; and to Storengy for permission to publish field data.

References

[1] B. Hugout, Mechanical behavior of salt cavities – in situ tests – model for calculating the cavity volume evolution, in: H.R. Hardy Jr., M. Langer (Eds.), Proceedings of the Second Conference on the Mechanical Behavior of Salt, Trans Tech Publications, Clausthal-Zellerfeld, Germany, 1988.
[2] P. Bérest, B. Brouard, M. Karimi-Jafari, L. Van Sambeek, Transient behavior of salt caverns. Interpretation of mechanical integrity tests, Int. J. Rock Mech. Min. Sci. 44 (2007) 767–786.
[3] U. Hunsche, Measurement of creep in rock salt at small strain rates, in: N.D. Cristescu, H.R. Hardy Jr, R.O. Simionescu (Eds.), Proceedings of the Fifth Conference on the Mechanical Behavior of Salt, Trans Tech Publications, Clausthal-Zellerfeld, Germany, 1999.
[4] D.E. Munson, K.L. De Vries, A.F. Fossum, G.D. Callahan, Extension of the Munson–Dawson model for treating stress drops in salt, in: M. Ghoreychi, P. Bérest, H.R. Hardy Jr, M. Langer (Eds.), Proceedings of the Third Conference on the Mechanical Behavior of Salt, Trans Tech Publications, Clausthal-Zellerfeld, Germany, 1996.
[5] P. Bérest, B. Brouard, Geometrical and rheological creep in salt caverns, in: L. Roberts, K. Mellegard, F. Hansen (Eds.), The Mechanical Behavior of Salt VIII, Taylor & Francis Group, London, 2015, pp. 199–208.